HERA Memo #111
Received 1 February 2022

The Impact of Simulator Choice and Parameterization on Fringe-Rate Signal Loss Calculations

Aaron Ewall-Wice

January 2022

Abstract

In this memo, we explore the impact of the choice of different visibility simulators on calculations of signal loss for fringe-rate filtering as a first step towards a more comprehensive analysis along the lines of [Aguirre et al., 2022] and [Kern et al., 2021]. We find very similar estimates for signal loss predictions are achieved between the pyuvsim‘ simulator package and vis_cpu and healvis simulators with their default settings, though $\approx 1\%$ time domain artifacts are prevalent in the pixelized beam prescription for vis_cpu which may motivate using higher beam pixelization or a different simulation. We also find that simulations with ~ 10000 sources (Nside=32) either randomly distributed or regularly spaced in a healpix grid give very similar results to ~ 300000 source simulations (Nside=128). Validation may find it expedient to run random fluctuations simulations at relatively low resolutions. We also observe spike-like artifacts in fringe-rate that are present only in healpix distributed source models but are not present in source models where the sources a distributed randomly.

1 The Simulations

We explore the impact of simulator choice on the signal loss for a single visibility in the HERA array at 155 MHz using four different simulation configurations listed in Table 2. We compare the pyuvsim[Lanman et al., 2019], healvis [Lanman et al., 2020], and vis_cpu[1] simulators. We also experimented with increasing the sampling resolution from every ≈ 100 seconds to every 10 seconds (4250 time samples instead of 425 time samples) and found this to have a negligible impact on our results. We use the CST Vivaldi beam located at `https://github.com/HERA-Team/HERA-Beams/blob/master/NicolasFagnoniBeams/NF_HERA_Vivaldi_efield_beam.fits` [Fagnoni et al., 2021] in all of our simulations. For our vis_cpu and pyuvsim simulations, we use the same source locations using the skyh5 format to pass the same consistent sky models between simulators. In all simulations, our sky model consists of discrete point sources either arranged on a healpix grid or randomly distributed with independently distributed fluxes drawn from an exponential distribution with a mean of two Jy. In our healvis simulation, the sources are drawn from a mean with two Jy / Sr. In all simulations, we use the baseline between antennas 91 and 92 in the HERA layout which is a 12 m EW and 8 m NS baseline.

In Fig. 1 we show the PSD in time at 155 MHz For the same baseline with various simulation choices. Most noteably, vis_cpu with its default settings is comprised of significant fringe-rate artifacts at the $\approx 10^{-3}$ level *in power*. For the other simulators, we observe differences between the various simulation prescriptions at the sub 1% level. In the regularly gridded healvis simulations for the NN pol, we see spike artifacts at ± 1.5 mHz for the NSide=32 simulation which appear at larger fringe-rates and at a lower level the Nside=128 simulation. These same spikes appear with larger amplitudes in the vis_cpu run. While pyuvsim agrees fairly well both healvis resolutions, the interpolated vis_cpu PSD is skewed at the 10^{-4} level. Another interesting aspect from these simulations is that none are free of artifacts that the 10^{-8} level so advances in simulation fidelity will be required validate time-domain techniques that must suppress systematics by greater than a factor of 10^4 level from visibilities

[1] `https://github.com/HERA-Team/vis_cpu.git`

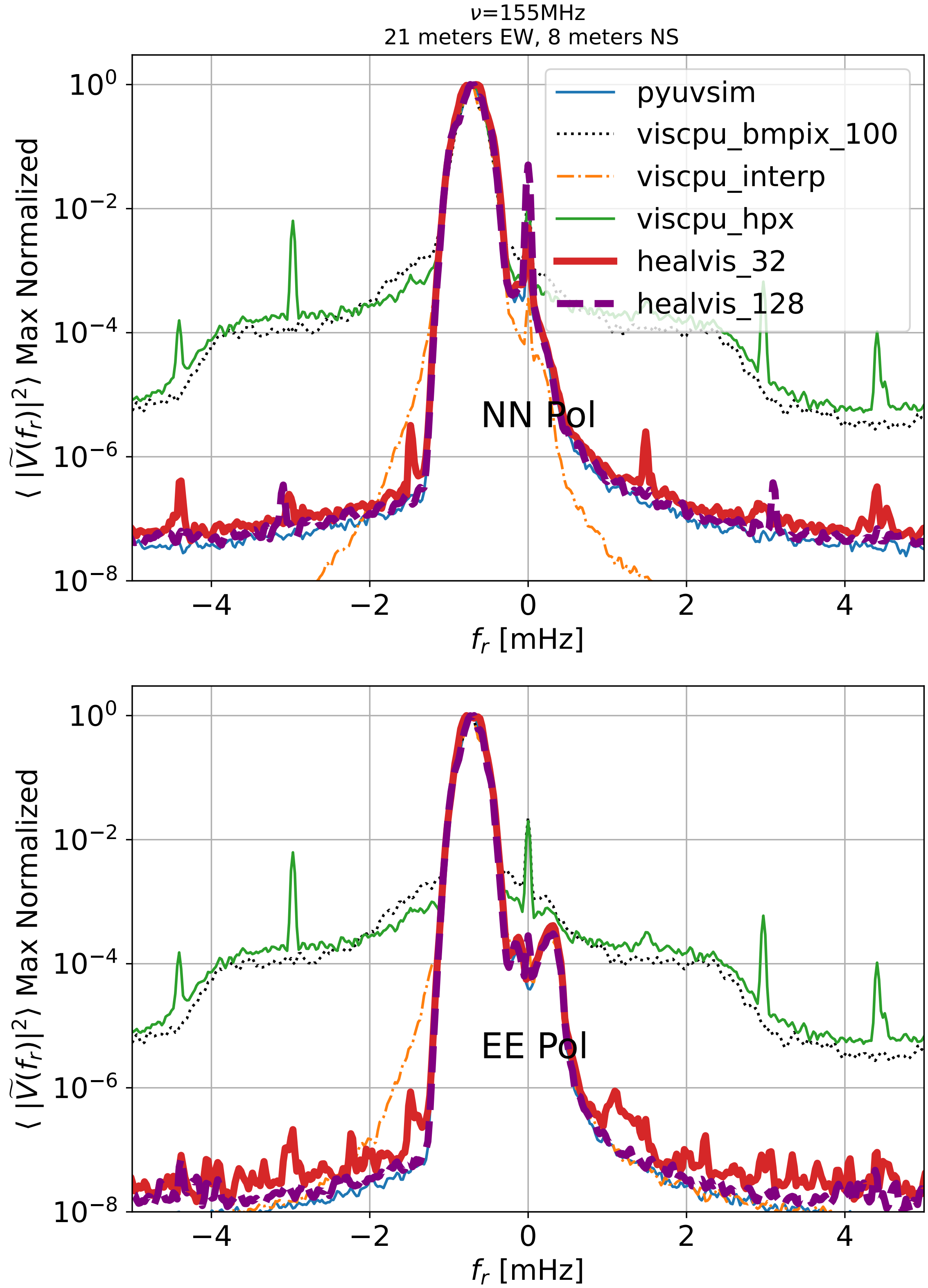

Figure 1: Averaged PSD over two-hundred independent simulations in the fringe-rate domain for our various simulator choices. We see that substantial wings exist for our pixelized beam vis_cpu runs. We also see that the healvis nside=128 and healvis nside=32 yield similar fringe-rate profiles (the nside=32 profile is slightly wider) so we may get away with lower resolution simulations with $\approx 10k$ sources.

Parameter	Value
Time Resolution	100 s
Fringe Rate Filter Standoff	0.05 mHz
Minimum Fringe Rate Filter Half Width	0.15 mHz
Lower histogram percentile for Fringe-Rate Limits	5%
Upper histogram percentile for Fringe-Rate Limits	95%
Number of Draws	200

Table 1: Common simulation and fringe-rate filtering parameters shared by all simulations. We found that using the full time resolution of the HERA observations of 10 s did not have a substantial effect on our results. Hence we stick with simulations with 100 s time resolution in this memo.

label	simulator	locations	matched?	Nsources	beam values
healvis_128	healvis	healpix	No	196608	healpix
healvis_32	healvis	healpix	No	12288	healpix
viscpu_bmpix_100	vis_cpu	uniform random	yes	12288	100×100 ortho
viscpu_interp	vis_cpu	uniform random	yes	12288	uvbeam interp
viscpu_hpx	vis_cpu	healpix	no	12288	u100×100 ortho
pyuvsim	pyuvsim	uniform random	yes	12288	uvbeam interp

Table 2: Parameters for our different simulation models. All simulations with 12288 sources and random source locations used the same sky model (indicated by the "matched" column. Our healvis simulations use sources distributed at healpix pixel positions. We draw the flux of each source from an exponential distribution with a mean of 2 Jy.

2 Fringe Rate Filtering

We perform fringe-rate filtering by fitting time-domain slepian sequences to the data in time [Ewall-Wice et al., 2021, Slepian, 1978] using the select_main_lobe branch of hera_cal which can be found at `https://github.com/HERA-Team/hera_cal/pull/736`. This allows us to extract a rectangular region in fringe-rate space with maximal power concentration. To set this rectangular region, we histogram the amplitude of the primary beam squared on an equal-area healpix grid against instantaneous fringe-rates on the sky [Parsons and Backer, 2009, Parsons et al., 2016] and set upper and lower limits set by the 5% and 95% limits of the CDF of these beam squared histograms. We also add a small 0.05 mHz offset to these limits and set the minimum half width of our filter to be 0.15 mHz to account for time structures arising from the spatial variations in the primary beam. To avoid polarization confusion, we include both the NN and EE polarized beams in the histogram step so that the same filter which includes both pols, is applied to both polarizations.

We show the residuals of our visibility after applying the fringe-rate filter in FR-space (Fig. 2) and time-space (Fig. 3). With the exception of vis_cpu the residuals all lie on a similar level in fringe-rate space.

3 Signal Loss

To evaluate the level of signal loss in our measurements, we compute the retained power ratio

$$R_{ret} = \frac{\sum_t |V_{frf}(t)|^2}{\sum_t |V(t)|^2} \tag{1}$$

where $V(t)$ is the visibility without fringe-rate filtering and $V_{frf}(t)$ is the fringe-rate filtered visibility (DPSS components fitted to the data in time).

In Fig. 4 we show histograms of R_{ret} for our various simulators. We find that all simulation options recover the median and 68% confidence intervals within several percent. The fiducial filter setting achieves a median signal loss of 5% with 84% of instances yielding signal loss below 10% or so. We note that the distributions for Nside=128 and Nside=32 are quiet close to eachother with relatively small differences in

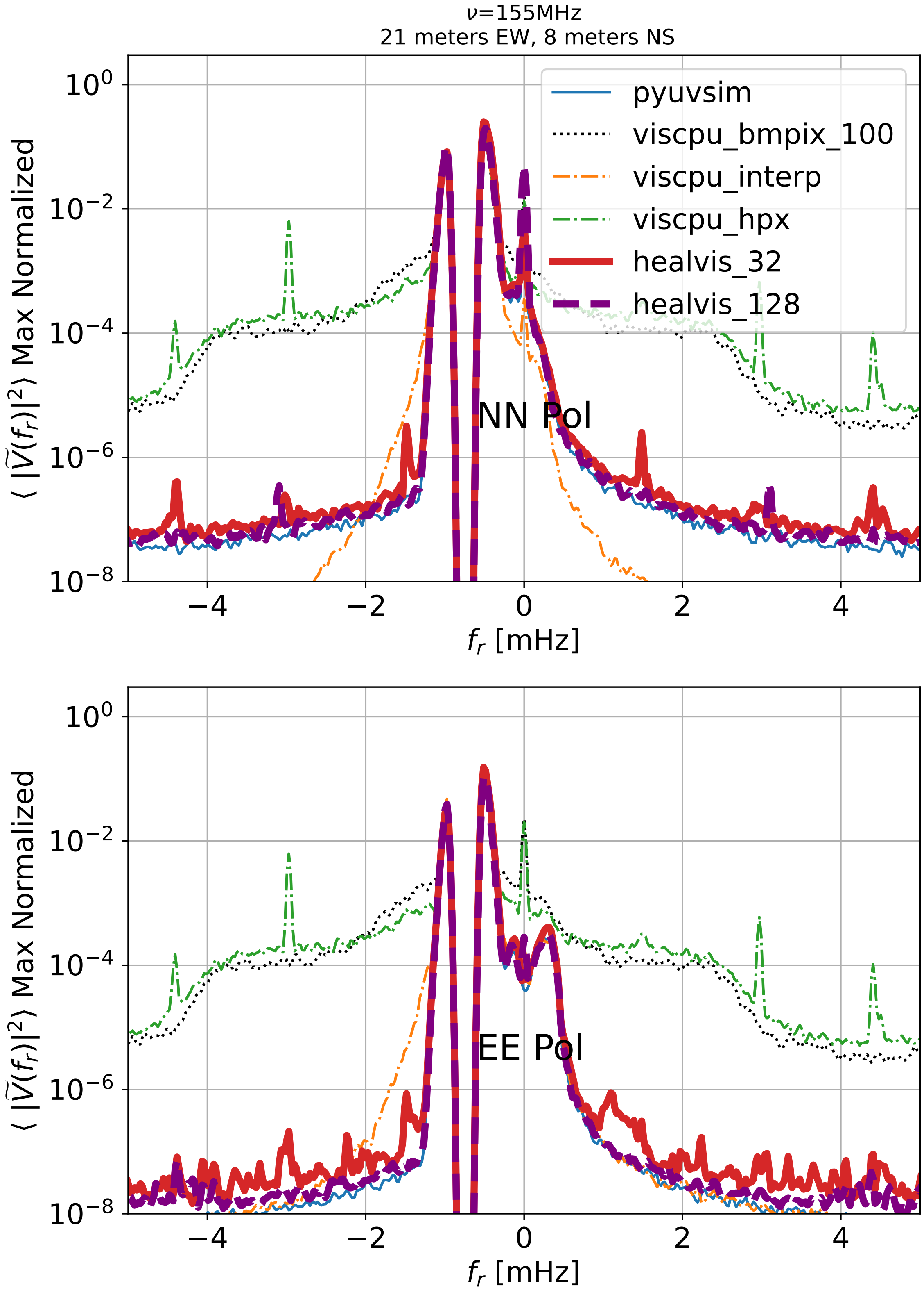

Figure 2: The same as Fig. 2 except after applying a fringe-rate filter designed to removed.

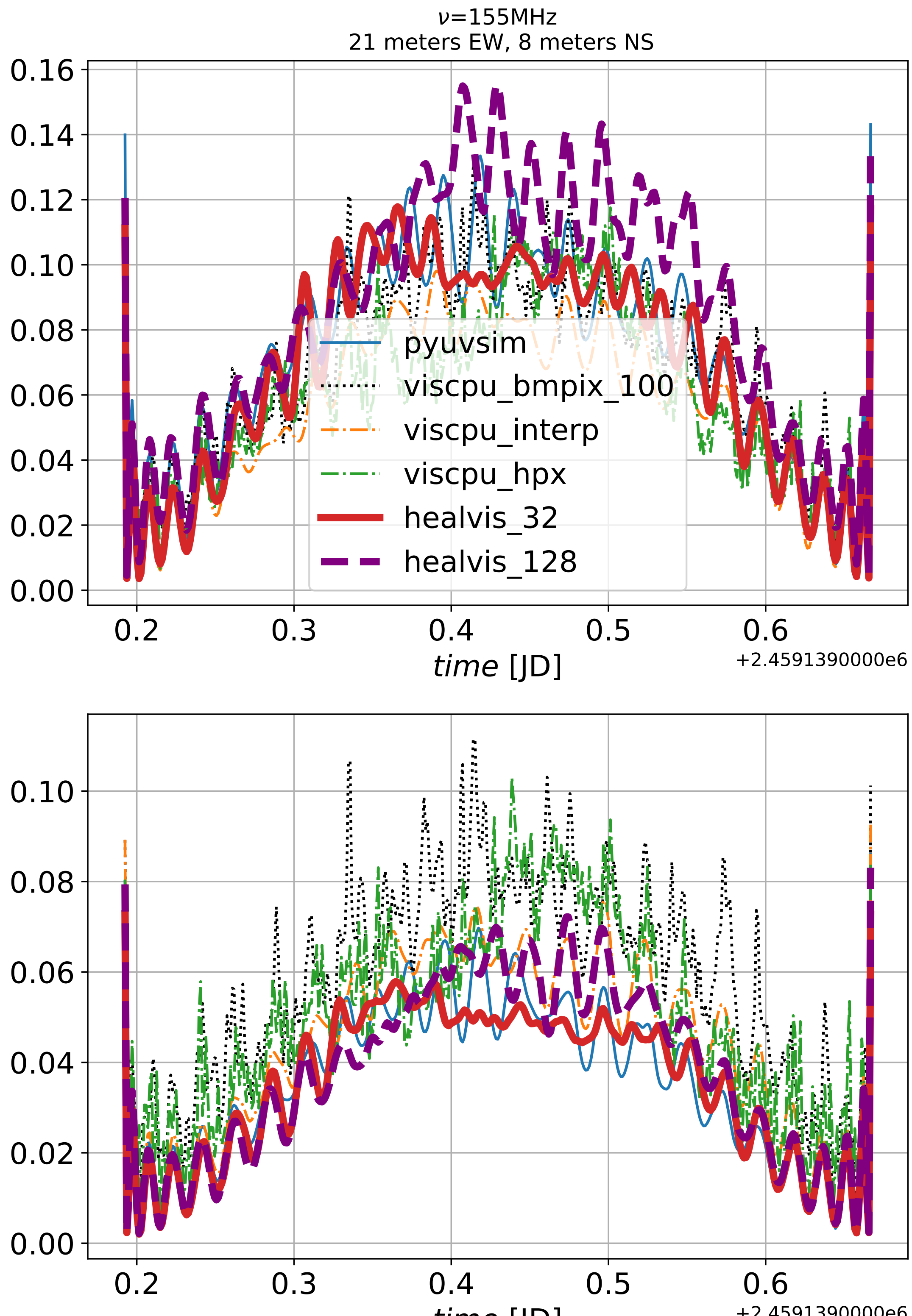

Figure 3: Mean of absolute value squared residuals over time, normalized to the mean square of the unfiltered data. **Top: NN** pol, **Bottom: EE** pol.

the modes and medians (a few percent) so it may be computationally advantageous to use simulations with only $\approx$ 10k sources rather then 300k.

4 A longer baseline

So far, we have only considered a relatively short baseline (twenty-two meters) to demonstrat convergence between different simulators and source count/resolution choices. However, we expect pixelization effects arising pixelization to be more prominant in long baselines. To consider this, we also explore the baseline between antennas 0 and 128 which has a 13 meter EW component and a 97 meter NS component.

In Fig. 5 we compare averages of the PSD for baseline 0-128 We do not repeate this experiment for pyuvsim due to run-time constraints. We find that the Nside=32 and Nside=128 Healvis runs are in very good agreement.

References

James E. Aguirre, Steven G. Murray, Robert Pascua, Zachary E. Martinot, Jacob Burba, Joshua S. Dillon, Daniel C. Jacobs, Nicholas S. Kern, Piyanat Kittiwisit, Matthew Kolopanis, Adam Lanman, Adrian Liu, Lily Whitler, Zara Abdurashidova, Paul Alexander, Zaki S. Ali, Yanga Balfour, Adam P. Beardsley, Gianni Bernardi, Tashalee S. Billings, Judd D. Bowman, Richard F. Bradley, Philip Bull, Steve Carey, Chris L. Carilli, Carina Cheng, David R. DeBoer, Matt Dexter, Eloy de Lera Acedo, John Ely, Aaron Ewall-Wice, Nicolas Fagnoni, Randall Fritz, Steven R. Furlanetto, Kingsley Gale-Sides, Brian Glendenning, Deepthi Gorthi, Bradley Greig, Jasper Grobbelaar, Ziyaad Halday, Bryna J. Hazelton, Jacqueline N. Hewitt, Jack Hickish, Austin Julius, Joshua Kerrigan, Saul A. Kohn, Paul La Plante, Telalo Lekalake, David Lewis, David MacMahon, Lourence Malan, Cresshim Malgas, Matthys Maree, Eunice Matsetela, Andrei Mesinger, Mathakane Molewa, Miguel F. Morales, Tshegofalang Mosiane, Abraham R. Neben, Bojan Nikolic, Aaron R. Parsons, Nipanjana Patra, Samantha Pieterse, Jonathan C. Pober, Nima Razavi-Ghods, Jon Ringuette, James Robnett, Kathryn Rosie, Mario G. Santos, Peter Sims, Saurabh Singh, Craig Smith, Angelo Syce, Nithyanandan Thyagarajan, Peter K. G. Williams, Haoxuan Zheng, and HERA Collaboration. Validation of the HERA Phase I Epoch of Reionization 21 cm Power Spectrum Software Pipeline. , 924(2):85, January 2022. doi: 10.3847/1538-4357/ac32cd.

Aaron Ewall-Wice, Nicholas Kern, Joshua S. Dillon, Adrian Liu, Aaron Parsons, Saurabh Singh, Adam Lanman, Paul La Plante, Nicolas Fagnoni, Eloy de Lera Acedo, David R. DeBoer, Chuneeta Nunhokee, Philip Bull, Tzu-Ching Chang, T. Joseph W. Lazio, James Aguirre, and Sean Weinberg. DAYENU: a simple filter of smooth foregrounds for intensity mapping power spectra. , 500(4):5195–5213, January 2021. doi: 10.1093/mnras/staa3293.

Nicolas Fagnoni, Eloy de Lera Acedo, Nick Drought, David R. DeBoer, Daniel Riley, Nima Razavi-Ghods, Steven Carey, and Aaron R. Parsons. Design of the New Wideband Vivaldi Feed for the HERA Radio-Telescope Phase II. *IEEE Transactions on Antennas and Propagation*, 69(12):8143–8157, December 2021. doi: 10.1109/TAP.2021.3083788.

Nicholas Kern, Scott Dynes, Honggeuen Kim, Jacqueline Hewitt, Eleanor Rath, Nicolas Fagnoni, Eloy De Lera Acedo, and David DeBoer. Hera memo 96: Time correlations of eor signals for hera with vivaldi feeds. `http://reionization.org/manual_uploads/HERA096_Fringerates_beamperturb.pdf`, 2021.

Adam Lanman, Bryna Hazelton, Daniel Jacobs, Matthew Kolopanis, Jonathan Pober, James Aguirre, and Nithyanandan Thyagarajan. pyuvsim: A comprehensive simulation package for radio interferometers in python. *The Journal of Open Source Software*, 4(37):1234, May 2019. doi: 10.21105/joss.01234.

Adam E. Lanman, Jonathan C. Pober, Nicholas S. Kern, Eloy de Lera Acedo, David R. DeBoer, and Nicolas Fagnoni. Quantifying EoR delay spectrum contamination from diffuse radio emission. , 494(3):3712–3727, May 2020. doi: 10.1093/mnras/staa987.

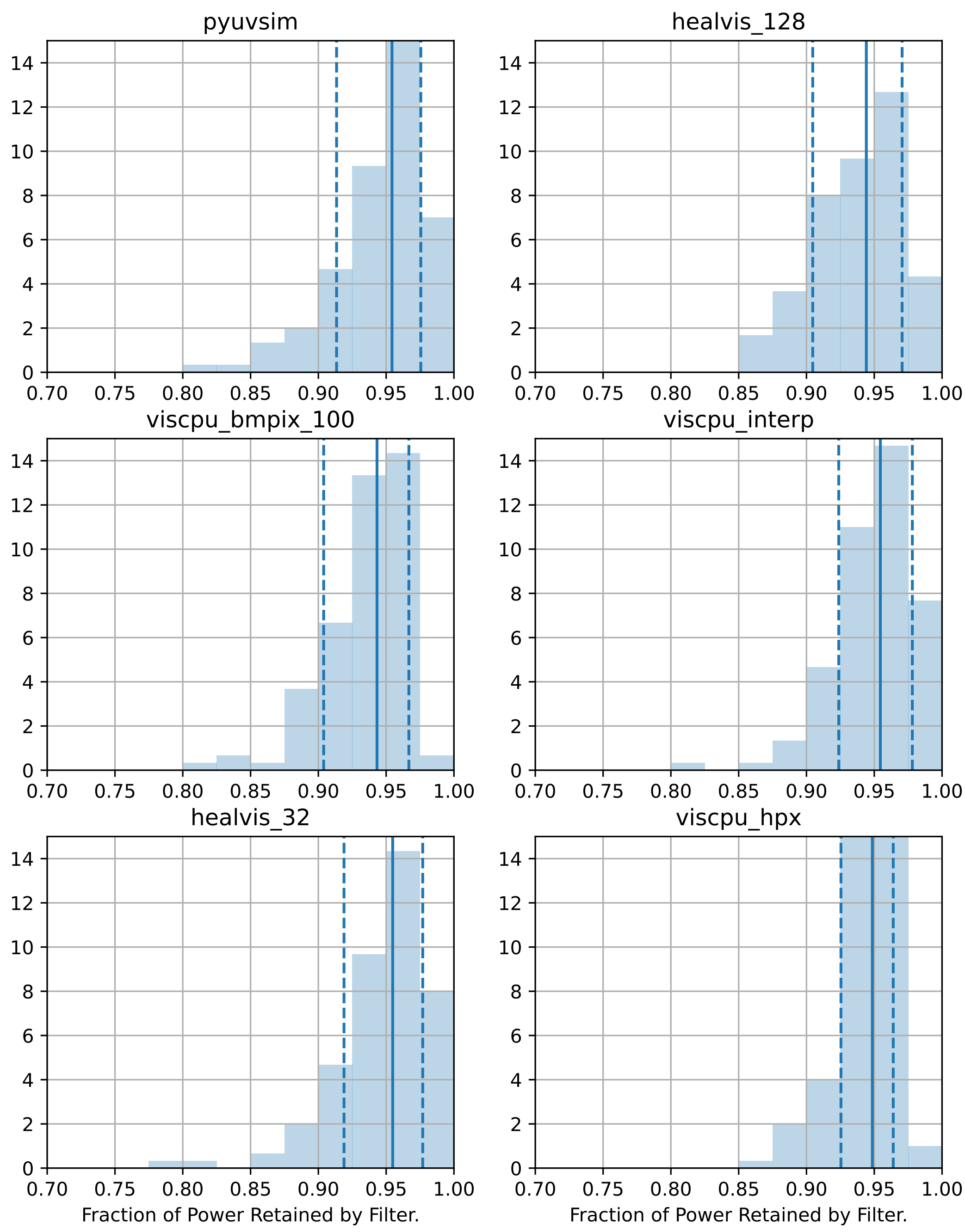

Figure 4: Distributions of signal retention for the fringe-rate filter on a 21 m EW 8 m NS baseline at 155 MHz. Vertical solid line indicates the median of the distributins and dashed vertical lines indicate the 68% confidence intervals for the retained power, R_{rt}

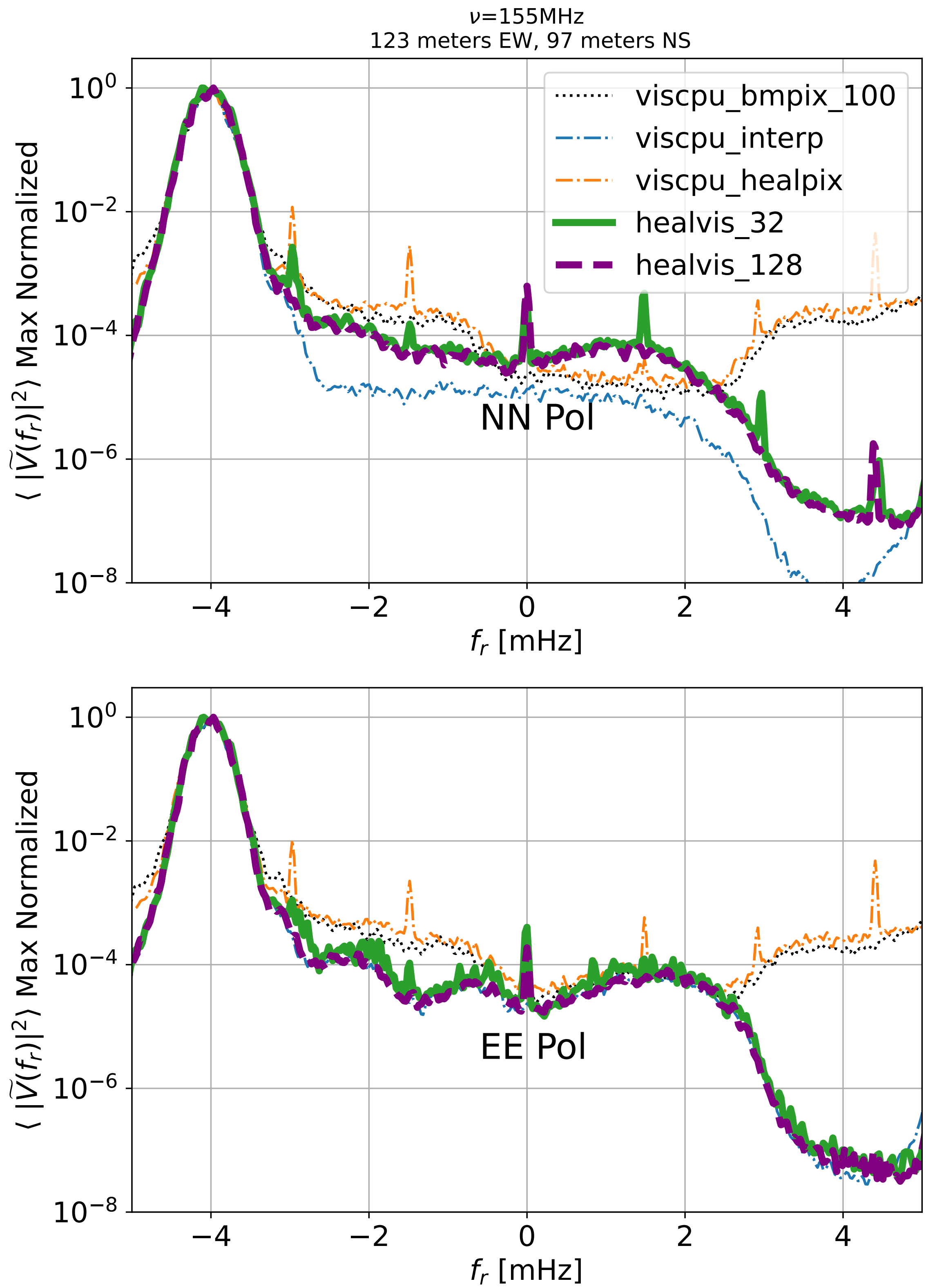

Figure 5: Same as Fig. 1 except now using the visiblity formed from antennas 0 and 128; a 123 meter EW, 97 meter NS baseline. Nside=32 and Nside=128 pixel counts are still relatively close together for healvis.

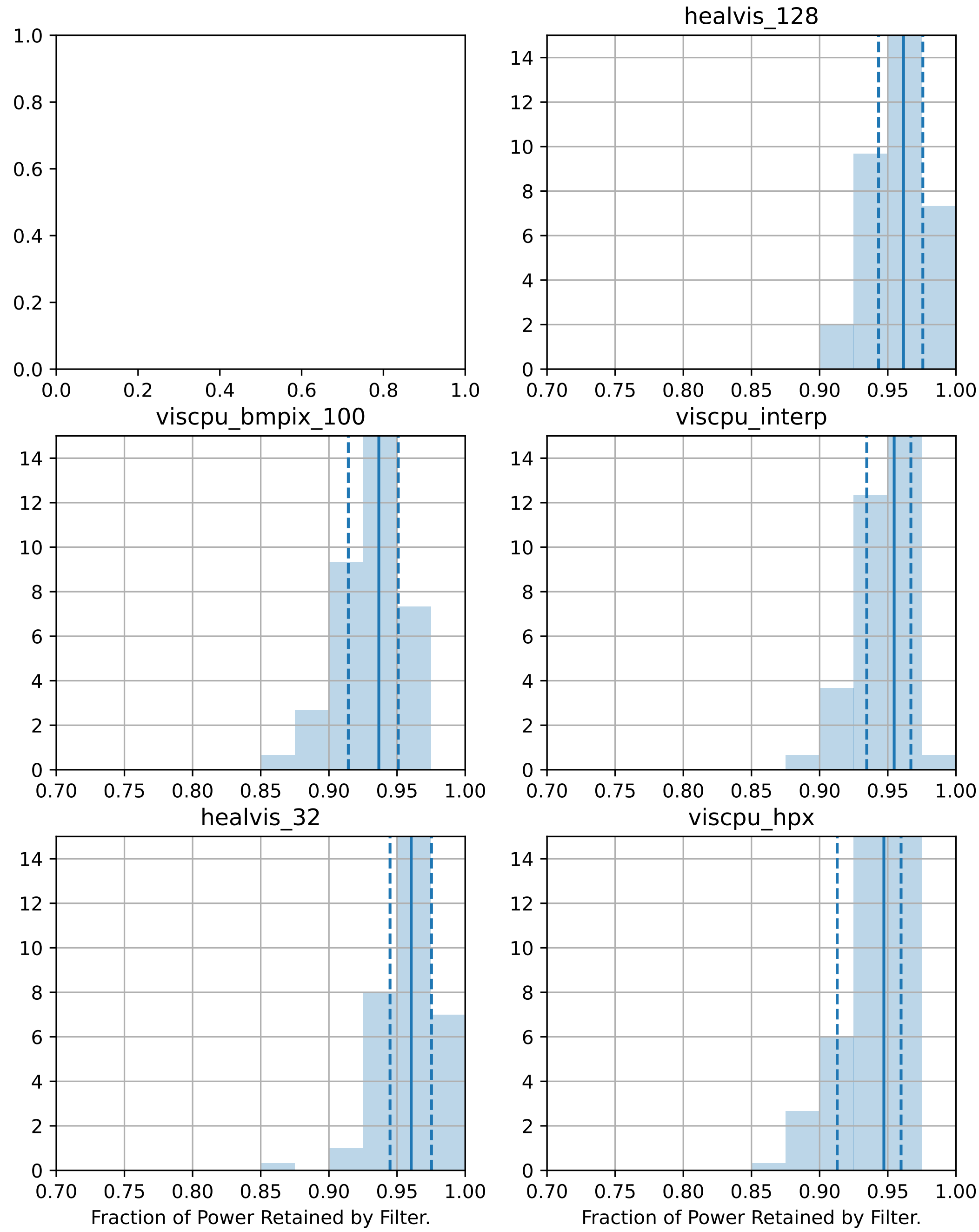

Figure 6: Same as Fig. 4 but now for a 123 meter EW and 97 meter NS baseline.

Aaron R. Parsons and Donald C. Backer. Calibration of Low-Frequency, Wide-Field Radio Interferometers Using Delay/Delay-Rate Filtering. , 138(1):219–226, July 2009. doi: 10.1088/0004-6256/138/1/219.

Aaron R. Parsons, Adrian Liu, Zaki S. Ali, and Carina Cheng. Optimized Beam Sculpting with Generalized Fringe-rate Filters. , 820(1):51, March 2016. doi: 10.3847/0004-637X/820/1/51.

D. Slepian. Prolate spheroidal wave functions, Fourier analysis, and uncertainty. V - The discrete case. *AT T Technical Journal*, 57:1371–1430, June 1978.